Journal of The Electrochemical Society

The Electrochemical Society
Advancing solid state & electrochemical science & technology

OPEN ACCESS

# Through-Plane Conductivity of Anion Exchange Membranes at Sub-Freezing Temperatures—Hydroxide vs (Bi-)Carbonate Ions

To cite this article: Jan N. Schwämmlein *et al* 2020 *J. Electrochem. Soc.* **167** 084513



*Journal of The Electrochemical Society*, 2020 **167** 084513

# Through-Plane Conductivity of Anion Exchange Membranes at Sub-Freezing Temperatures—Hydroxide vs (Bi-)Carbonate Ions

**Jan N. Schwämmlein,[1,*,z] Nhat Long T. Pham,[1] Thomas Mittermeier,[1,**,a] Masamitsu Egawa,[1] Lukas Bonorand,[2,b] and Hubert A. Gasteiger[1,***]**

[1]*Chair of Technical Electrochemistry, Department of Chemistry and Catalysis Research Center, Technical University of Munich, Lichtenbergstraße 4, D-85748 Garching, Germany*
[2]*Electrochemistry Laboratory, Paul Scherrer Institut, CH-5232 Villigen PSI, Switzerland*

Anion exchange membrane fuel cells (AEMFCs) are considered as potential future alternative for proton exchange membrane fuel cells (PEMFCs) due to their potential to not require platinum. However, many properties of alkaline ionomers/membranes are not yet well-characterized. The goal of this study is to evaluate the suitability of current AEMs for application in a wide range of operating conditions, especially at temperatures below the freezing point of water. For this, a method was developed to reversibly convert the counter ion of the cationic group in the membrane electrode assembly (MEA) from (bi-)carbonate to hydroxide and vice versa. Subsequently, the through-plane membrane conductivity in an AEMFC was evaluated by electrochemical impedance spectroscopy at different temperatures (−20°C to 50°C) and water contents, whereby the electrical resistance contribution (contact and through-plane) to the high frequency resistance of the cell was determined in an ex-situ experiment. The results obtained in this study were compared to a standard PEM (Nafion 212) and to a sulfonic acid based membrane with a hydrocarbon backbone. The here acquired conductivity data suggest that the conductivity of the evaluated anion exchange membrane, particularly in its (bi-) carbonate form, would be too low at sub-zero temperature to meet automotive freeze start requirements.
 [DOI: 10.1149/1945-7111/ab8cdf]

Manuscript submitted December 10, 2019; revised manuscript received March 1, 2020. Published May 7, 2020.

For the envisaged transition to decarbonize the fuel cycle, $H_2$ powered fuel cells are a promising candidate to play a major role, e.g., for automotive applications. Proton exchange membrane fuel cells (PEMFCs) are currently being rolled-out to the (mass) market by multiple car manufacturers.[1–3] However, a major hurdle for a widespread implementation of PEMFCs is their need for noble metal catalysts to drive the hydrogen oxidation reaction (HOR) and the oxygen reduction reaction (ORR). While the high HOR kinetics enable ultra-low Pt loadings in PEMFCs,[4] the sluggish kinetics of the ORR on platinum or platinum alloy catalysts,[5,6] require the utilization of at least 100 $\mu g_{Pt}$ $cm^{-2}$.[7] In contrast to the acidic environment in PEMFCs, several more abundant and affordable metals, such as Ag[8,9] or Ni,[10] exhibit sufficient stability as well as ORR activity in alkaline media, therefore enabling a wider choice of cathode catalysts.[11] On the other hand, the only sufficiently active catalysts for the HOR in alkaline media are platinum and platinum group metals (PGMs), but their HOR kinetics are approximately two orders of magnitude lower in alkaline compared to acidic medium, so that ultra-low PGM loadings cannot be used in fuel cells based on alkaline electrolytes.[12–16] Nevertheless, $H_2$-based fuel cells operating in alkaline media are an interesting technological concept and therefore a subject of frequent studies.[17,18]

An increased interest in this technology was triggered by the development of membranes carrying cationic groups to conduct hydroxide ions instead of protons, enabling the construction of alkaline fuel cells using anion exchange membranes (AEMs) instead of an aqueous alkaline electrolyte. A general overview on different AEM types was presented by Merle et al.,[19] and the most recently developed materials are summarized by Gottesfeld et al.[18] and Fan et al.[20] Even though significant progress has been made to improve the properties of AEMs, their conductivity is still significantly lower compared to conventional PEMs,[18] in part due to the roughly 2-fold lower mobility of hydroxide ions ($20.6 \cdot 10^{-8}$ $m^2$ $s^{-1}$ $V^{-1}$) compared to protons ($36.2 \cdot 10^{-8}$ $m^2$ $s^{-1}$ $V^{-1}$) in dilute aqueous solutions at 25°C.[21] Especially when exposed to ambient air containing $CO_2$, the ionic conductivity of anion exchange membranes decrease significantly upon the reaction of the hydroxide ions with $CO_2$ to (bi-)carbonate,[18,21–23] consistent with the roughly 3–4 times lower mobility of carbonate ($7.5 \cdot 10^{-8}$ $m^2$ $s^{-1}$ $V^{-1}$) and bicarbonate ($4.6 \cdot 10^{-8}$ $m^2$ $s^{-1}$ $V^{-1}$) ions compared to hydroxide ions. Up to now, the conductivity of alkaline membranes was subject of various studies with respect to the conducting species,[23,24] the relative humidity (*RH*)[23,25] and the temperature[22,24] within the typical operating range of a fuel cell, especially focusing on temperatures between 60°C–80°C. With respect to automotive applications, however, starting-up of the fuel cell system at ambient or sub-zero degree temperatures is important and was thoroughly studied for PEMs,[26] but to the best of our knowledge never looked into for AEMs.

Hence, the focus of the present study is to evaluate the conductivity of an anion exchange membrane at sub-freezing conditions in both its hydroxide and its (bi-)carbonate form. To enable the exchange of the ionic group between hydroxide and (bi-)carbonate, a measurement methodology was developed where the membrane was hot-pressed with two symmetrical electrodes based on Pt/C and assembled in a conventional single fuel cell testing setup consisting of the MEA, sandwiched between gas diffusion layers (GDLs), flow fields, and end plates. To change the water content of the membrane in a defined and reproducible manner, the MEAs were equilibrated at 50°C with gases humidified at different relative humidities. Subsequently, the wet gas atmosphere was removed by a short purge (75 s) with dry gas, after which the cell was sealed and subjected to a freeze cycle down to ca. −15°C (starting at 50°C) followed by a thaw cycle (back up to 50°C). During these freeze/thaw cycles, the high frequency resistance (*HFR*) was measured; the membrane resistivity was determined by subtracting the ex-situ determined electrical resistance from the *HFR* (both given as areal resistance, accounting for the membrane area) and by dividing the resulting membrane areal resistance by the dry membrane thickness (membrane conductivity is thus the reciprocal of this number). It shall be mentioned at this point that the thickness of the membrane is expected to vary depending on the conditions (especially *RH* and temperature), but we consider the estimate of the membrane conductivity via the dry membrane thickness a suitable approach to determine representative numbers. The removal of liquid water

*Electrochemical Society Student Member.
**Electrochemical Society Member.
***Electrochemical Society Fellow.
[a]Present address: e.GO:REX GmbH, Aachen, Germany.
[b]Present address: SMT Energy AG, 8952 Zurich-Schlieren, Switzerland.
[z]E-mail: jan.schwaemmlein@tum.de

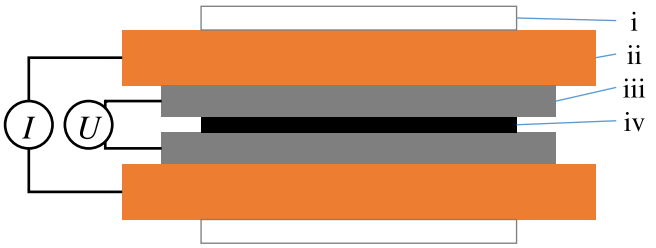


**Figure 1.** Experimental setup for the determination of the electrical resistance of the cell assembly by a four-point probe measurement. While the current (*I*) was applied to the copper plates (ii), the resulting voltage drop (*U*) was measured directly at the graphite flow fields (iii). The assembly, placed into a hydraulic press, was isolated by expanded PTFE sheets (i), and two gas diffusion layers with microporous layers facing each other (iv) were placed between the flow fields.

from the gas flow channels by a short purge (short enough to not significantly change the water content in the membrane) is crucial to avoid water condensation in the flow field channels and to obtain a defined water content in the membrane (as described in the Experimenal section). To validate the here described method to obtain low-temperature membrane conductivities for water contents defined by equilibration at 50°C, the conductivity of a well-known PEM (Nafion 212) was evaluated between +50°C and −20°C, comparing the obtained values with those reported in the literature. Subsequently, this measurement method was applied to a sulfonic acid based membrane with a hydrocarbon backbone (furtheron referred to as HC-PEM) as comparison (further information on radiation-grafted HC-PEMs are given by Albert)[27] and finally to a commercially available AEM (Tokuyama A201) in both its hydroxide and (bi-)carbonate form. The conductivity of the HC-PEM in this study is given as a reference to the data measured on the AEM, since the polymer backbone of both the AEM and the HC-PEM are fluorine-free and hydrocarbon based, which is very different from the perfluorinated backbone of Nafion. As had been shown in the literature before (e.g., C. K. Mittelsteadt and H. Liu),[28] the water uptake of all sulfonic acid based membranes (both fluorine-free and perfluorosulfonic acid (PFSA) based membranes) is essentially identical at ⩽80% RH (see Fig. 1 in Ref. 28) and only differs at >80%, while the drop of conductivity with decreasing *RH* is in all instances more pronounced for hydrocarbon based membranes compared to PFSAs (see Fig. 4 in Ref. 28). The latter feature applies to all sulfonic acid based HC-PEMs compared to PFSAs, even though there still is a large difference in conductivity at a given *RH* for different hydrocarbon backbones and side-groups. Therefore, while the conductivity vs. *RH* relationship differs between different HC-PEMs, HC-PEMs with a flurorine-free backbone do represent a class of materials with generally different properties from membranes with perfluorinated backbones. For this reason we believe that the comparison of a specific HC-PEM with the AEM does indeed provide interesting new information, despite the fact that there is no "standard" HC-PEM in the way Nafion represents a "standard" PFSA membrane and Tokuyama A201 represents a "standard" AEM.

## Experimental

All potentials given in this manuscript refer to the measured voltage versus the counter/reference electrode (i.e., 100% $H_2$ on a dry gas basis) if not otherwise stated. Pressures are given as absolute pressures, measured and controlled at the inlet of the fuel cell. All gasses were of high purity (grade 5.0), supplied by *Westfalen AG* (Germany). Gas flows are given in nccm, referenced to 0°C at a pressure of 101.3 kPa.

***MEA preparation.***—All fuel cell tests were executed with 50 $cm^2$ active-area MEAs, fabricated by the decal transfer method. PEM-based MEAs consisted of a standard Pt/C catalyst at a loading of 100 $\mu g_{Pt}\ cm^{-2}$ on each side, and an ionomer to carbon (I/C) ratio of ≈1/1 $g_I \cdot g_C^{-1}$, applying a standard Nafion ionomer. Details regarding hot pressing of PEM-based MEAs can be obtained from earlier publications (155°C, 0.11 kN $cm^{-2}$, 3 min).[29,30] MEAs consisting of a Nafion 212 membrane (50 $\mu$m thickness, 1.0 meq $g^{-1}$, QuinTech e.K., Germany) and of the sulfonic acid based membrane with a hydrocarbon-based backbone (HC-PEM, 30 $\mu$m thickness, 1.6–1.7 meq $g^{-1}$) were prepared the same way.

The preparation of the HC-PEM was based on the radiation grafting technique and involved three steps, viz., irradiation, grafting, and sulfonation. A 25 $\mu$m thick ethylene-co-tetrafluoroethylene base film (ETFE, Tefzel LZ-100, *Du Pont Corp.*, USA) was electron irradiated (2.5 MeV, *Leoni AG*, Switzerland) with a dose of 15 kGy and subsequently stored at −80°C until used. Grafting was carried out at a temperature of 55°C in a solution of 30%$_v$ monomer, 55%$_v$ isopropanol (technical, *Merck Millipore KGaA*, Germany), and 15%$_v$ ultrapure water (18.2 MΩ cm, *Merck Millipore KGaA*, Germany) for 24 h. The monomer was a mixture of $\alpha$-methylstyrene (99%, *Sigma Aldrich Corp.*, Germany) and acrylonitrile (⩾99%, *Sigma Aldrich Corp.*, Germany) with a molar ratio of 2.5 to 1.0. Sulfonation of the grafted films was carried out in a solution of 10%$_v$ chlorosulfonic acid (99%, *Sigma Aldrich Corp.*, Germany) in dichloromethane (technical, *Merck Millipore KGaA*, Germany) at room temperature for 6 h, followed by hydrolysis of the sulfonyl chloride groups in deionized water at 80°C for 8 h. The ion exchange capacity was determined via titration and the water uptake was determined based on the difference in mass between the wet and the dry membrane. To ensure that all ionic groups within the hydrocarbon membrane carried protons, MEAs prepared with the HC-PEM were treated in 5%$_v$ $H_2SO_4$ at 80°C for 12 h, followed by repeated cleaning (3 times, at least 1 h, each) with ultrapure water. Thereafter, the MEAs were left to dry in ambient air and stored in dry state until assembled.

AEMs consisted of a Tokuyama A201 membrane (28 $\mu$m thickness, ca. 1.7 meq $g^{-1}$, *Tokuyama Corp.*, Japan), a commercial 50%$_{wt.}$ Pt/C catalyst (TEC10V50E, *Tanaka Kikinzoku Kogyo K.K.*, Japan) and the FAA-3 ionomer (solid ionomer sheet in the $Br^-$ ion form, *Fumatech GmbH*, Germany) at an I/C ratio of 0.8/1.0 $g_I \cdot g_C^{-1}$. Catalyst inks for AEMs were prepared by mixing the catalyst with the ionomer dispersion, comprised of 10%$_{wt}$ $H_2O$ and 90%$_{wt}$ 2-propanol (Chromasolv Plus, 99.9%, *Sigma Aldrich Corp.*, Germany). The catalyst, followed by the solvent mixture, was added into a 15 ml capped bottle (HDPE), already containing 15 g of $ZrO_2$ beads (5 mm, *Glen Mills Inc.*, USA) in $N_2$ atmosphere. To obtain a suitable viscosity for the coating process, the carbon content of the ink was adjusted to 50 $mg_C\ ml^{-1}$, resulting in a total solid content of ≈15%$_{wt}$. The inks were mixed by placing the bottles onto a roller-mill (60 rpm) for 24 h at room temperature. Thereafter, the ink was coated on etched FEP (extruded, *Angst+Pfister GmbH*, Switzerland) using the Mayer rod technique with the appropriate bar on an automated coating machine. AEM-based MEAs were prepared by hot pressing the membrane between two electrode decals at 110°C for 10 min with an applied force of 1 kN $cm^{-2}$, using a polymer foil (Kapton, *Du Pont Corp.*, USA) to protect the MEA and foamed PTFE (Gylon Style 3545 Soft, *Garlock GmbH*, USA) to distribute the pressure equally over the entire MEA area. The platinum content of the two electrodes was determined by weighing the decals before and after the hot pressing procedure. Both electrodes in the MEAs were identical with a loading of 400 ± 40 $\mu g_{Pt}\ cm^{-2}$. To assure a complete exchange of the anion exchange membrane/ionomer with (bi-)carbonate ions, the MEAs were ion exchanged three times in 1 M $Na_2CO_3$ (anhydrous, for analysis, *Sigma Aldrich Corp.*, Germany) solution for at least 24 h each, and subsequently washed three times by placing them in ultrapure water for at least 30 min. Thereafter, the MEAs were left to dry in ambient air and stored in dry state until assembled.

***Electrical resistance measurements.***—The electrical areal resistance ($R_{electr.}$) of the cell assembly, used for the determination of the

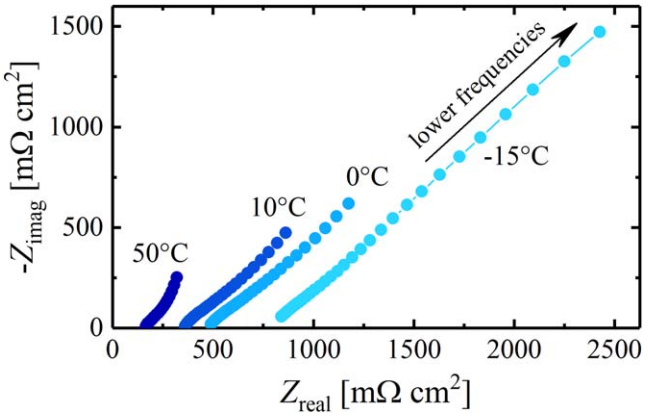


**Figure 2.** Exemplary Nyquist plot showing the negative imaginary part of the impedance ($-Z_{imag}$) versus the real part ($Z_{real}$) for an MEA comprising a Tokuyama A201 membrane in the hydroxide form (the procedure to convert the membrane from (bi-)carbonate to hydroxide form is discussed below) recorded at different temperatures, after the MEA had been equilibrated at 50°C and 80% *RH*. The impedance spectra were recorded with both electrodes under $N_2$ (i.e., in $N_2/N_2$ configuration) at zero DC current, with an AC current perturbation of 3 mA $cm^{-2}$ from 500 kHz to 100 Hz.

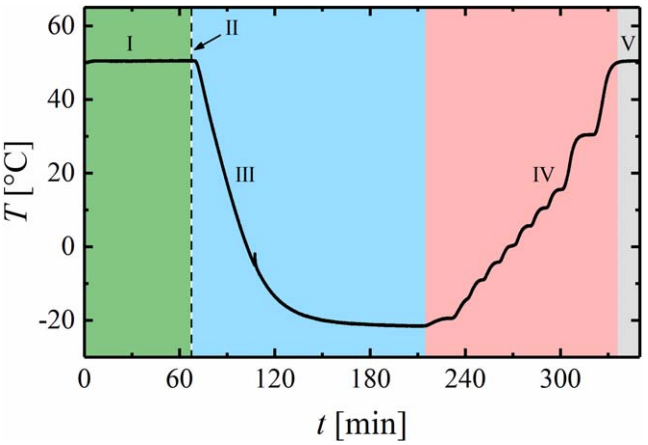


**Figure 3.** Exemplary profile of the cell temperature, *T*, versus time, *t*, showing a full freeze-thaw cycle after equilibration of the MEA at 50°C. Phase I: equilibration of the MEA (green area); phase II: dry gas purge (dashed line); phase III: freeze cycle (blue area); phase IV: thaw cycle (red area); phase V, constant temperature phase for reference (grey area).

membrane conductivity, was acquired by a four-point probe measurement in the absence of a membrane. The schematic setup is depicted in Fig. 1, composed of (i) isolating, expanded PTFE (Gylon Style 3545 Soft, *Garlock GmbH*, USA), providing a homogeneous pressure distribution; (ii) two polished copper plates; (iii) two graphite flow fields (*Fuel Cell Technologies, Inc.*, USA) with 0.79 mm wide and 1.02 mm deep channels separated by 0.80 mm wide lands, and arranged in 10 serpentines with 4 channels each; and, (iv) two 50 $cm^2$ GDLs (Sigacret 25BC, *SGL Carbon GmbH*, Germany) with the microporous layers (MPLs) facing each other. To measure the electrical resistance of this configuration, a constant current of $I = 3$ A was applied via a standard laboratory power supply connected to the polished copper plates (ii in Fig. 1), and the resulting voltage drop, *U*, was measured by a digital voltmeter (Fluke 289, *Fluke Corp.*, USA) at additional contacts inserted into the graphite flow fields (iii in Fig. 1). Thus, the electrical areal resistance. was calculated as $R_{electr.} = \frac{U}{I} \cdot 50\,cm^2$. To determine the pressure dependency of $R_{electr.}$, the pressure was increased by a hydraulic platen press (modified P 200 PM, *Dr Collin GmbH*, Germany) in several steps until a total pressure of 2 MPa was reached (based on the total active area, i.e., 10 kN for the 50 $cm^2$ GDLs). All measurements to determine the electrical resistance were performed at 30°C, whereby the temperature was assumed to be negligible (experiments between 30°C–80°C at 2 MPa compression indicated a linear behavior of $R_{electr.}$ with temperature corresponding to 0.04 mΩ $cm^2°C^{-1}$, which is negligible over the here considered temperature range). To evaluate the pressure distribution in the actual cell setup, a cell was assembled with all components (including an MEA), placing pressure sensitive dye paper (Prescale Super Low, *Fujifilm Corp.*, Japan) directly on top of the MEA.

***Cell conditioning and conductivity measurements.***—The measurements to determine the membrane conductivity at different temperatures and different membrane humidification were performed on an in-house manufactured single-cell 50 $cm^2$ hardware, whereby the endplates were fitted with internal coolant channels to enable a uniform thermal control of the cell with a coolant (1:1 mixture of ethylene glycol and deionized water) whose temperature was controlled by an external thermostat (FP50-HL, Julabo GmbH, Germany). Commercial graphite flow fields (0.79 mm channel and 0.80 mm land width; see above) were used with anode and cathode gases directed in counter-flow configuration. The GDL (see above) compression was adjusted to 20 ± 1% by PTFE-coated quasi-incompressible fiberglass gaskets (Fiberflon, Fiberflon GmbH & Co. KG, Germany), and the cell was assembled at a torque of 12 Nm (for details see Simon et al.).[31] Cell conditioning and conductivity tests were performed on automated test stations (G60, Greenlight Innovation Corp., Canada) equipped with a potentiostat (Reference 3000, Gamry Instruments, USA) to conduct electrochemical impedance spectroscopy (EIS). After an initial conditioning procedure (see below), impedance spectra were recorded on $N_2$ purged cells ( i.e., both electrodes under $N_2$, furtheron referred to as $N_2/N_2$ configuration) at zero DC current, with an AC current perturbation of 3 mA $cm^{-2}$ from 500 kHz to 100 Hz. The HFR was extracted as *x*-axis intersect in a Nyquist plot and multiplied with the active area of 50 $cm^2$ to obtain an areal resistance. For measurements which did not show an *x*-axis intersect at the highest frequency (e.g., at −15°C, Fig. 2), the straight line at high frequencies was extrapolated to $Z_{imag} = 0$ mΩ $cm^2$. The exemplary Nyquist data shown in Fig. 2 for the case of an AEMFC equilibrated at 50°C and 80% RH exhibits a slope of ≈45° at high frequencies, bending off towards a more vertical direction at low frequencies. This represents the initial part of a purely capacitive transmission line model for the ion conduction in the electrodes in the absence of reactive gas. Details about the transmission line model can be found elsewhere (e.g., Liu et al.).[32]

The conductivity of all membranes was determined between approximately −20°C and +50°C, after the MEAs had been equilibrated at 50°C with humidified $N_2$ (between 20%–100% *RH*) flowing through both cell compartments (500/500 nccm $N_2/N_2$ at 150 $kPa_{abs}$) for 70 min (Fig. 3, phase I). Before initiating the resistance measurements, liquid water in the gas channels of the cell was removed by a 75 s long dry gas purge (Fig. 3, phase II) with $N_2/N_2$ at a flow rate of 50 nccm on each side; as will be outlined below, the total amount of $N_2$ flowing through the cell during this period was chosen such that the amount of membrane dry-out is negligible. Directly after this purge, the gas supply and outlet valves of the cell were closed and the gas stream was interrupted. Then, the cell was subjected to a freeze cycle, slowly cooling it from +50°C to the desired temperatures (Fig. 3, phase III), followed by a thaw cycle during which the temperature is gradually increased again to +50°C (Fig. 3, phase IV). The heating period consisted of several intermediate target temperatures, (resulting in similar freeze- and thaw times. The EIS was measured periodically throughout the entire freeze-thaw cycle and the temperature change during the measurement (<30 s per EIS measurement) can be neglected. Finally, the cell was maintained at +50°C to measure the conductivity after an entire freeze-thaw cycle, allowing for a comparison with the initial value (Fig. 3, phase V).

In the following, we will estimate the maximum error of the membrane water content introduced by the dry gas purge step

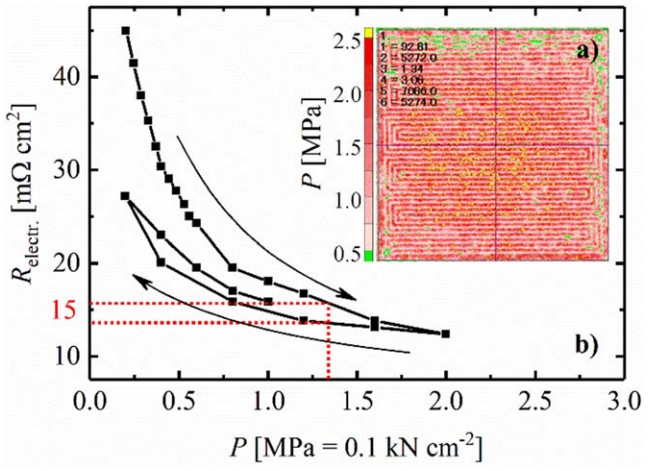


**Figure 4.** (a) Ex-situ pressure distribution determined for the cell configuration shown in Fig. 1. (b) Electrical resistance, $R_{\text{electr.}}$, as a function of the pressure, $P$, applied onto the end plates, showing a first compression cycle and a first compression release cycle (marked by arrows), as well as a second compression cycle (data in between the first compression and the first compression release cycle). The measurement was conducted with a four-point probe in DC mode at 30°C (see Fig. 1).

performed after each equilibration at 50°C with $N_2$ humidified at different *RH* values. The maximum water uptake from the membrane into the gas volume during the purge procedure can be calculated according to the definition of relative humidity (Eq. 1) for the applied total $N_2$ flow rate (100 nccm, i.e., 50 nccm on each side) and purge time (75 s). Assuming that the *RH* at the exit of the cell has a maximum value equal to the *RH* adjusted during the preceding equilibration phase (Fig. 3, phase I), i.e., assuming that the membrane water content and the gas flow are always in equilibrium (representing the maximum loss of water from the membrane; we assume that the MEA actually requires a certain amount of time to adjust to the gas atmosphere, causing an even lower measurement error), the *RH* can be linked to a maximum water loss during the dry gas purge:

$$RH = \frac{p_{H_2O}}{p^{sat}_{H_2O}} = \frac{n_{H_2O}}{n_{H_2O} + n_{dry}} \cdot \frac{p}{p^{sat}_{H_2O}} \quad [1]$$

In this, $n_{H_2O}$ is the molar quantity of water in the $N_2$ gas exiting the cell, $p^{sat}_{H_2O}$ is the vapor saturation pressure of water (12.34 kPa at 50°C), $n_{dry}$ is the dry gas quantity calculated from the nitrogen flow rate and purge time ($n_{dry} = 5.6$ mmol) and $p$ is the gas pressure during the purge (150 $kPa_{abs}$). Equation 1 can be solved for $n_{H_2O}$, which represents the maximum total amount of water which will be removed from the membrane (strictly speaking from the MEA) during the dry gas purge period.

$$n_{H_2O} = n_{dry} \cdot \frac{p^{sat}_{H_2O} \cdot RH}{p - p^{sat}_{H_2O} \cdot RH} \quad [2]$$

For example, at an *RH* of 100% at 50°C ($p_{H_2O} = 12.35$ kPa), the water content in a Nafion membrane can be calculated according to Eq. 1 from Mittelsteadt and Liu,[28] resulting in a membrane water content of $\lambda = 10$ (with $\lambda$ defined as $mol_{H_2O}\, mol^{-1}_{SO_3^-}$). For a membrane area of 50 $cm^2$, a thickness of 50 $\mu$m, a density of 2 g $cm^{-3}$, and an ion exchange capacity of ≈1 meq $g^{-1}$, the total amount of $H_2O$ contained in the membrane at $\lambda = 10$ is 5 mmol. On the other hand, the maximum water uptake into the gas stream according to Eq. 2 is ≈0.5 mmol, which is minor compared to the amount of water stored in the membrane. Analogously, at an $RH = 20\%$, the calculated maximum water loss through the dry gas purge is $n_{H_2O} \approx$ 0.1 mmol compared to 1 mmol of $H_2O$, initially stored in the membrane (based on a membrane water content of $\lambda = 2$ at 50°C and 20% *RH*).[28] Hence, the $\lambda$ value reached during the equilibration phase can be considered to remain approximately constant (with a maximum loss of membrane water content of ≈10%) over the course of the dry gas purge, rendering the here presented method suitable to determine the conductivity of membranes with a well-controlled water content at temperatures below the freezing point of water. The same estimates can be made for the AEM and for the HC-PEM, resulting in similar maximum water loss fractions, as the membranes have a similar thickness and essentially the same ion exchange capacity when reference to membrane volume (i.e, in terms of meq $cm^{-3}$). During cool-down (and subsequent thaw), the water content can be safely assumed to remain constant, due to the limited locked-in gas volume in the cell (≈2.8 $cm^3$) and low saturation vapor pressure, as already discussed by Tajiri et al.[33]

In experiments with AEM based MEAs, the membrane and ionomer was converted from the (bi-)carbonate form into the hydroxide form via an electrochemical pre-treatment prior to equilibration at 50°C and at the desired *RH*. For this, the cell was operated with 500/500 nccm of $H_2/O_2$ at 80% *RH*, 150 $kPa_{abs}$, and 50°C for ≈1 min at a cell voltage of 100 mV. The associated current allowed to convert the entire ionomer in the MEA into the hydroxide form by migration of all contained (bi-)carbonate species to the anode and releasing them as $CO_2$ via the exhaust gas. Afterwards, the cell conditioning and the *HFR* measurements were performed as described above. For measurements in the carbonate form, following the initial $H_2/O_2$ conditioning, air at the respective humidity of the subsequent measurement was flown on both sides of the cell for ≈2 h (note that the $H_2$ compartment was initially purged with $N_2$ to avoid damage due to gas fronts of $H_2$ and air), whereby the $CO_2$ content in the air (≈400 ppm) is sufficiently high to convert essentially all hydroxide ions into (bi-)carbonate ions.[34] Subsequently, the gases were switched to $N_2/N_2$ in order to equilibrate the water content of the MEA prior to initiating the freeze-thaw cycle.

## Results and Discussion

***Electrical resistance.***—A common measure for the ohmic resistance of a fuel cell setup is the so-called *HFR*, which can be determined from the intersect of the impedance with the real axis of a Nyquist plot obtained by EIS (Fig. 2). As the *HFR* is a measure of the total ohmic resistance in the PEMFC, it is commonly expressed as the sum of the contact/bulk electrical resistance of flow fields, GDLs and electrodes ($R_{\text{electr.}}$) plus the ionic resistance of the membrane ($R_{\text{membrane}}$). $R_{\text{electr.}}$ is mainly dependent on the chosen experimental setup (e.g., applied contacting pressure, flow field, and GDL type) and is essentially independent of the ionic resistance of the membrane, which strongly depends on *RH* and, to a lesser degree on temperature. Therefore, in order to obtain the resistance contribution from the membrane, $R_{\text{electr.}}$ needs to be subtracted from the *HFR*; from the thus obtained value for $R_{\text{membrane}}$, the conductivity of the membrane can be calculated. Since an in-situ determination of the electrical resistance is challenging, an ex-situ experiment was conducted to determine its magnitude. In this four-point probe setup, a constant current (3 A) was applied to the current collectors and the voltage was measured at the flow fields (Fig. 1). To determine the dependency of the electrical resistance on the applied pressure, the setup was placed in a hydraulic press and exposed to a compression/expansion cycle at 30°C, with a maximum effective pressure of 2 MPa (i.e., 10 kN applied on the 50 $cm^2$ GDL area). As shown in Fig. 4b, the measured electrical resistance decreased with increasing applied pressure, reaching a minimum of ≈12 mΩ $cm^2$ (at 2 MPa); this compression dependence of $R_{\text{electr.}}$ is well-documented in the literature (e.g., Mathias et al.).[35] A hysteresis of $R_{\text{electr.}}$ was found when the pressure was reduced again, with the measured resistance at the lowest compression being clearly lower than what was obtained prior to the first compression process. $R_{\text{electr.}}$ during the second compression cycle coincides closely with that obtained

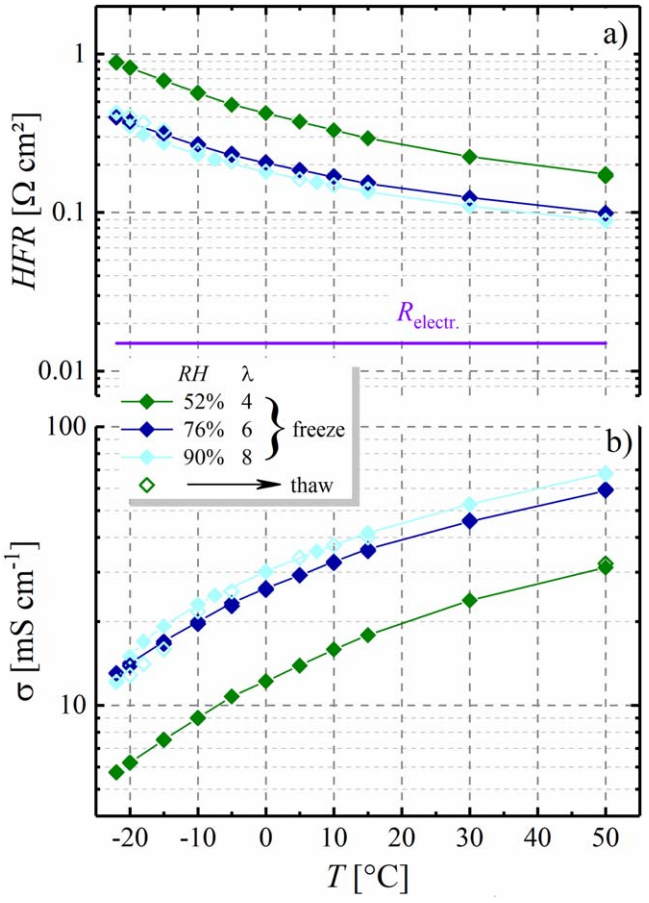


**Figure 5.** (a) *HFR* of an MEA with a Nafion 212 membrane as a function of temperature and water content, defined by equilibration of the MEA at 50°C in humidified $N_2$ streams (RH values of 52%, 76%, and 90%, corresponding to $\lambda = 4$, 6, and 8, respectively). The freeze cycle is shown as full symbols and hollow symbols represent the thaw cycle (note that these are mostly overlapping). The estimated electrical resistance, $R_{electr.}$, for the cell set-up is given for comparison by the horizontal purple line (within the accuracy of these measurements it is assumed to be independent of *RH* and temperature). (b) Through-plane conductivity of the membrane as a function of the temperature, calculated by subtraction of $R_{electr.}$ from the measured *HFR* and by normalization to the thickness of the membrane (50 $\mu$m), according to Eq. 3.

during the first compression release cycle, indicating that irreversible compression (in the literature referred to as residual strain) was triggered mostly during the initial compression process. To determine the approximate electrical resistance in the actual cell assembly with which the conductivity measurement are conducted (i.e., the same assembly but with the MEA inserted between the GDLs), the pressure in the actual cell setup used for freeze/thaw conductivity measurements was evaluated by a pressure distribution test using pressure sensitive dye paper. As shown in Fig. 4a, the pressure distribution over the entire active area (i.e., the GDL area) reflects the flow field structure with higher compressive stress under the land areas than under the channels. The average value over the total 50 $cm^2$ was determined to be ≈1.3 MPa (the images were scanned with a Epson Perfection V33 and analyzed with the provided software), where Fig. 4b reveals a value of $R_{electr.} \approx 15 \pm 3$ mΩ $cm^2$. Therefore, the electr resistance $R_{electr.}$ which we used to correct all *HFR* values in order to obtain $R_{membrane}$ was 15 mΩ $cm^2$ (cf, Eq. 3); considering that this value is ≈7 times lower than the lowest *HFR* values measured in our entire study (≈90 mΩ $cm^2$; see Fig. 5), we consider the error produced by the estimated variation in the actual $R_{electr.}$ value of ca. ±3 mΩ $cm^2$ to be negligible.

***Conductivity measurement method verification with Nafion 212.—***Prior to evaluating the conductivity of membranes of interest, we will first validate our here proposed method to quantify the low-temperature through-plane membrane conductivity at various well-defined membrane humidification levels. This will be done by means of comparative measurements with a Nafion 212 membrane whose conductivity is well-known over a wide range of temperatures. The Nafion 212 MEAs were equilibrated at 50°C with $N_2$ flowing through both sides of the cell ($N_2/N_2$ at 500/500 nccm) that was humidified at 52%, 70%, and 90% *RH*, which corresponds to membrane water contents of and $\lambda = 4$, 6, and 8, respectively (based on the correlation by Mittelsteadt and Liu).[28] After this membrane equilibration, followed by a short dry $N_2$ gas purge and subsequent sealing of the cell under $N_2/N_2$, the cell temperature was first decreased to −22°C (freeze cycle) and then increased again (thaw cycle) to the initial value of +50°C. During the freeze/thaw cycles, the *HFR* was determined at different temperatures from the high frequency intercept of the impedance spectra with the *x*-axis in a Nyquist plot (see, e.g., Fig. 2). These data are shown in Fig. 5a for the freeze cycle (solid symbols) and for the thaw cycle (hollow symbols) for an MEA utilizing a conventional Nafion 212 membrane. As mentioned above, the ex-situ estimated electrical resistance contribution ($R_{electr.}$, drawn as a purple line in Fig. 5a and considered to be independent of *RH* and temperature within the accuracy of these measurements) is substantially smaller than the lowest *HFR* of 90 mΩ $cm^2$ measured in this study (namely for the Nafion 212 MEA equilibrated at 50°C and 90% *RH* (≡$\lambda = 8$); see light blue line in Fig. 5a). Therefore, the here described measurement methodology is considered sufficiently accurate to evaluate the ionic resistance of the membrane by means of subtracting the electrical resistance from the *HFR*. However, it has to be mentioned that the thus determined membrane resistance and conductivity are most precise for high *HFR* values, hence at low temperatures and/or *RH*. Owing to the strong temperature and *RH* dependence of the membrane resistance,[28] the measured *HFR* increases substantially with decreasing temperature and *RH*. No significant differences are observed between the *HFR* values determined during the freeze cycle (closed symbols in Fig. 5a) compared to those obtained during the subsequent thaw cycle (open symbols; indeed, the data points are mostly overlapping), confirming that the water content of the membrane remained unchanged during the entire freeze-thaw cycle experiment.

After subtraction of the electrical resistance contribution of $R_{electr.} \approx 15$ mΩ $cm^2$, the conductivity of the membrane can be calculated according to Eq. 3, where $\sigma$ is the conductivity (in S $cm^{-1}$) and $d$ is the thickness of the membrane (in the dry state).

$$\sigma = \frac{d}{HFR - R_{electr.}} \quad [3]$$

The thus obtained conductivities of the Nafion 212 membrane are shown in Fig. 5b and can be compared to the values reported by Thompson et al.[36] for a Nafion 117 membrane with the same ion exchange capacity. At 20°C, these authors report conductivies ranging from 15–30 mS $cm^{-1}$ at $\lambda = 6$ and from 35–45 mS $cm^{-1}$ at $\lambda = 8$ and 20°C,[36] which are slightly lower, but in a comparable range as the ≈39 mS $cm^{-1}$ at $\lambda = 6$ and the ≈45 mS $cm^{-1}$ at $\lambda = 8$ shown in Fig. 5b. At −20°C and $\lambda = 8$, Thompson et al. report an average value of ≈12 mS $cm^{-1}$, which is also only slightly lower than the ≈14 mS $cm^{-1}$ obtained in our experiments at the same conditions. Based on this, we conclude that our method to determine the membrane conductivity at low temperatures and under defined humidification conditions a valid approach; the slight differences to the literature might be due to the fact that the membrane resistance measured by Thompson et al. is based on in-plane measurements while ours is based on through-plane measurements.

***Conductivity of an HC-PEM.—***As comparison for the conductivity measurements performed later on with an alkaline membrane,

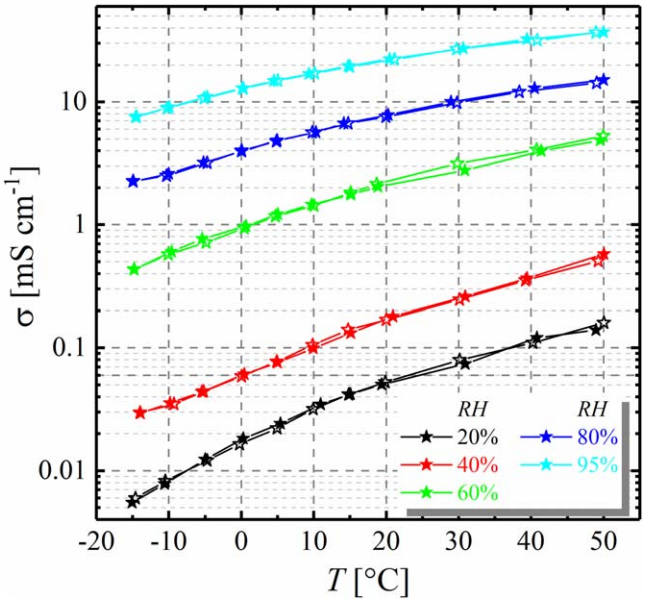


**Figure 6.** Through-plane conductivity, $\sigma$, of a sulfonic acid based membrane with a hydrocarbon backbone (referred to as HC-PEM) as function of temperature, $T$, for various water contents obtained by equilibration of the membranes at 50°C differently humidified gases (the corresponding *RH* values are given in the figure). $\sigma$ was calculated by subtraction of $R_{electr.}$ from the measured *HFR* and normalization to the thickness of the membrane (30 $\mu$m), according to Eq. 3. The freeze cycle is shown as full symbols, while hollow symbols represent the thaw cycle.

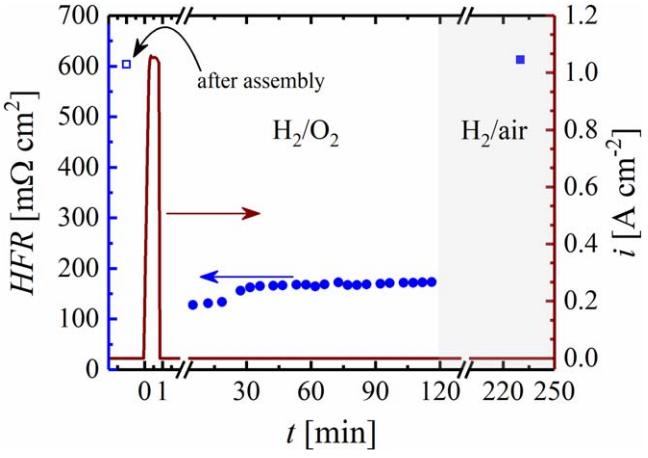


**Figure 7.** *HFR* of an MEA based on a Tokuyama A201 membrane (28 $\mu$m) in (bi-)carbonate form measured either directly after cell assembly with the carbonate exchanged membrane (labeled "after assembly", hollow blue square) or after the "carbonate purge" (see below) and a subsequent exposure to air (blue filled square). The carbonate purge which converts the (bi-) carbonate ions to hydroxide ions consists of applying a cell voltage of 100 mV in $H_2/O_2$ (at 500/500 nccm, 150 $kPa_{abs}$, 50°C, 80% *RH*) for ≈1 min (the brown line shows the current drawn during this period); the subsequently measured *HFR* in the hydroxide form is shown by the blue circles. The supplied gases, as marked in the figure, are either $H_2/O_2$ (directly after cell assembly and until t = 120 min) or $H_2$/air (starting at t = 120 min and continuing until t = 250 min; also at 500/500 nccm, 150 $kPa_{abs}$, 50°C, 80% *RH*).

the conductivity of a sulfonic acid based membrane with a hydrocarbon backbone (referred to as HC-PEM) was evaluated by the method validated above with Nafion 212. This is shown in Fig. 6, and as before no difference in the conductivity values obtained during the freeze cycle (solid symbols) and during the thaw cycle (open symbols) is observed. While Nafion is composed of a fully perfluorinated polymer backbone, having pendent aliphatic side chains, hydrocarbon-based sulfonic acid membranes typically consist of non-fluorinated polyaromatic units, containing hydrogen endgroups.[37] In general, hydrocarbon-based membranes are considered as an alternative for the commonly applied perfluorinated membranes due their lower production cost, a lower permeability towards $H_2$ and $O_2$, and possibly due to a higher creep resistance at high temperature. First of all, the conductivity of the here investigated hydrocarbon-based membrane at 50°C and high *RH* is almost 2-fold lower (37 mS $cm^{-1}$ for membrane equilibrated at 50°C and 95% *RH*; light blue line in Fig. 6) compared to the perfluorinated Nafion 212 membrane (68 mS $cm^{-1}$ for membrane equilibrated at 50°C and 90% *RH*; light blue line in Fig. 5b). This is even more pronounced at lower humidification levels, where the conductivity at 50°C of the HC-PEM is ≈6-fold lower (5 mS $cm^{-1}$ for membrane equilibrated at 50°C and 60% *RH*; green line in Fig. 6) compared to Nafion 212 membrane (30 mS $cm^{-1}$ for membrane equilibrated at 50°C and an even slightly lower *RH* of 52%; dark green line in Fig. 5 b).[38] Even more extreme differences develop when comparing the conductivities at −15°C at lower humidification levels, where HC-PEM conductivity (0.45 mS $cm^{-1}$ for membrane equilibrated at 50°C and 60% *RH*; green line in Fig. 6) is ≈17-fold lower than that of Nafion 212 (7.5 mS $cm^{-1}$ for membrane equilibrated at 50°C and an even slightly lower *RH* of 52%; dark green line in Fig. 5b). We assume that this is due to the fact that hydrocarbon membranes are commonly known to show a lower degree of phase separation between hydrophilic and hydrophobic domains due to (i) the lower hydrophobicity of the hydrocarbon backbone, (ii) the lower hydrophilicity of the sulfonic acid group on account of its lower acidity, and, (iii) the smaller flexibility of the aromatic structure due to steric hindrances (dependent on the type of hydrocarbon).[37] Therefore, the proton conducting hydrophilic network in hydrocarbon-based sulfonic acid membranes is more tortuous with narrower conduction channels and more dead-ends, causing a lower overall conductivity. This becomes especially evident at low water content (corresponding to low *RH* levels during the equilibration procedure at 50°C), which leads to a decrease of the network connectivity and therefore a strong decrease in conductivity, as illustrated by the above comparison. The lack of phase separation in hydrocarbon-based membranes was also reported by other researchers, e.g., by Ahn et al. who showed excellent $H_2$/air fuel cell performance at high humidity, but strong limitations for air supplied with an *RH* of 40%.[38] The origin of the apparently more significant decrease of the conductivity of the HC-PEM with temperature compared to Nafion 212 (most pronounced for low water content, as illustrated above) is, however, still unknown.

***Conductivity of an AEM.***—In contrast to the sulfuric acid group, commonly employed in PEMs, anion exchange membranes apply alkaline end groups on the side chain, e.g., based on quaternary ammonium ions, to conduct hydroxide ions through the ionomer phase of the AEMFC.[18,20,21] While pure $O_2$ is generally used for diagnostic purposes, the relevant cathode gas for practical fuel cell applications would be ambient air, which, however, contains approximately 400 ppm $CO_2$.[39] The latter was shown to react with the hydroxide ions in the ionomer phase to form (bi-)carbonate species.[21–23]

$$CO_2 + OH^- \rightarrow HCO_3^- \quad [4]$$

$$HCO_3^- + OH^- \rightarrow CO_3^{2-} + H_2O \quad [5]$$

In equilibrium with ambient air, the main ionic species present as counter ions of the anion exchange groups are carbonate and bicarbonate, with estimated mole fractions of 2/3 and 1/3, respectively.[40] For the remainder of this manuscript, the equilibrated mixture of carbonate and bicarbonate ions in the anion exchange membrane ionomer will be referred to as "(bi-)carbonate form" of

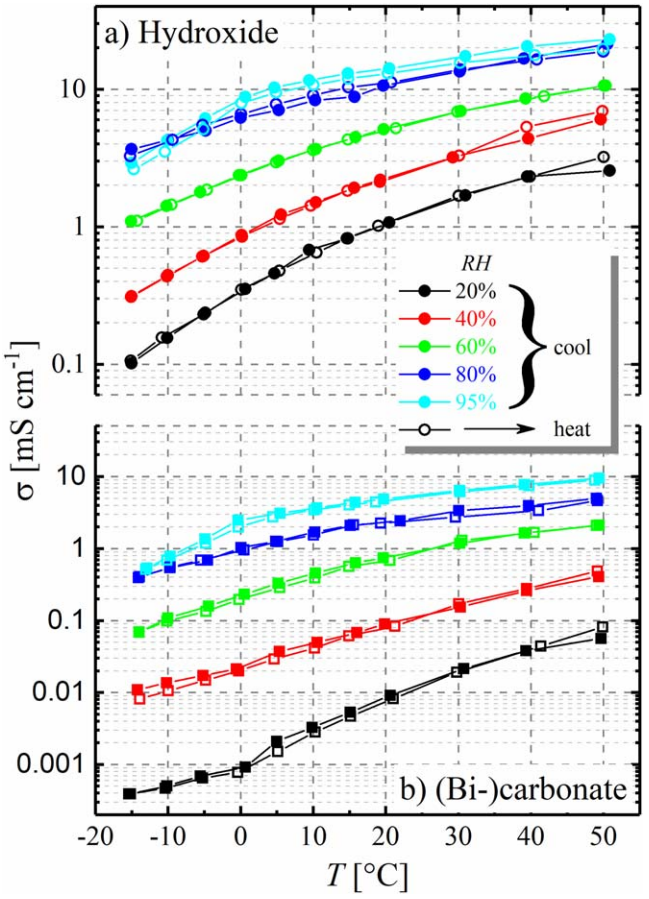


**Figure 8.** Through-plane conductivity, $\sigma$, of an MEA consisting of a Tokuyama A201 membrane equilibrated at 50°C with $N_2/N_2$ humidified at different *RH* values (as marked in the figure) as function of temperature, *T*, determined either in (a) the hydroxide form (circles) or in (b) the (bi-)carbonate form (squares). $\sigma$ was calculated by subtraction of $R_{electr.}$ from the measured *HFR* and normalization to the thickness of the membrane (28 $\mu$m), according to Eq. 3. The freeze cycle is shown as full symbols, while hollow symbols represent the thaw cycle. The hydroxide form was obtained by the carbonate purge approach described in Fig. 7, while the (bi-)carbonate form was obtained by a subsequent exposure to air/air.

the AEM. Since the neutralization of AEMs is inevitable upon exposure to ambient air, all alkaline MEAs were prepared directly in the carbonate form by exchanging all ionic groups in 1 M $Na_2CO_3$ solution. Compared to hydroxide ions ($20.6 \cdot 10^{-8}$ $m^2$ $s^{-1}$ $V^{-1}$), the mobility of carbonate ($7.5 \cdot 10^{-8}$ $m^2$ $s^{-1}$ $V^{-1}$) and bicarbonate ions ($4.6 \cdot 10^{-8}$ $m^2$ $s^{-1}$ $V^{-1}$) is rather low,[21] hence, membranes comprising mainly carbonate and bicarbonate ions provide a very limited ionic conductivity.[22,41]

In accordance, the *HFR* of an MEA directly after assembly and equilibration at 50°C and an *RH* of 80% (while supplying $H_2$ and $O_2$ to anode and cathode, respectively) was as high as 604 m$\Omega$ $cm^2$ (Fig. 7, blue hollow square). Upon drawing a large current, the membrane can be converted from carbonate to hydroxide form, since carbonate ions migrate to the anode side where they are released into the exhaust stream of the AEMFC as $CO_2$. As shown in Fig. 7 (brown line), the current increased rapidly to a maximum of ≈1 A $cm^{-2}$ when the cell voltage was set to 100 mV under these conditions. This current (±10%) was reproducibly reached in all experiments presented here; MEAs that suffered damage during testing, i.e., that provided a lower $H_2/O_2$ performance when setting the potential to 100 mV (termed "carbonate purge"), were not considered for the evaluation of the membrane conductivity. The *HFR* measured directly after the carbonate purge (Fig. 7, blue circles) was significantly lower (≈130 m$\Omega$ $cm^2$) compared to that measured after assembly, confirming the exchange of carbonate with hydroxide ions. No difference in the *HFR* was observed when the duration of the carbonate purge was prolonged (not shown), hence a short carbonate purge time of ≈1 min was chosen to avoid MEA degradation during the high current density application. A slight increase of the *HFR* was observed in the 30 min following the carbonate purge, which subsequently remained constant for another 90 min. We attribute the initial increase of the *HFR* after the carbonate purge to the equilibration of the membrane to the relative humidity condition supplied by the $H_2/O_2$ flows (80% *RH* in this figure), considering that the membrane water content during the high current density drawn during the carbonate purge is expected to be higher than in the absence of current. Furthermore, the fact that the *HFR* remained constant for more than 90 min verifies that the cell setup utilized for the experiments presented here is sufficiently sealed from ambient air, preventing the gradual change of the membrane from hydroxide to (bi-)carbonate form which would occur upon ambient air intrusion. To convert the membrane back to the (bi-)carbonate form in a controlled experiment, the oxygen supply was replaced by ambient air (containing ≈400 ppm $CO_2$). After an equilibration period of approximately two hours, the *HFR* increased to the same value as was obtained directly after assembly (compare solid and open blue squares in Fig. 7), confirming the full conversion into the (bi-)carbonate form. Hence, measurements of the membrane conductivity in the (bi-)carbonate form were performed in the following order: carbonate purge to ensure that the MEA yielded the desired performance, followed by an exchange to the (bi-)carbonate form by air exposure in the fuel cell system for two hours. Apart from the ion exchange procedure, conductivity measurements of AEMs were conducted according to the procedure developed for Nafion 212.

As expected, the conductivity of the Tokuyama A201 membrane was significantly lower in the (bi-)carbonate (Fig. 8b) compared to the hydroxide form (Fig. 8a), e.g., at 50°C it is 5 mS $cm^{-1}$ compared to 19 mS $cm^{-1}$ for the membrane equilibrated at 50°C and 80% *RH* (dark blue lines). The approxima0tely 3–4 times higher conductivity of the hydroxide compared to the carbonate form is in good alignment with that expected from the difference of the ionic mobility (≈3.2, assuming 2/3 carbonate and 1/3 bicarbonate), and similar factor which had been reported previously based on in-plane conductivity measurements of the membrane in liquid water.[22] This again confirms that the measurements aiming to determine the conductivity of the membrane in the hydroxide form were not influenced by the intrusion of $CO_2$ from the outside. Compared to Nafion 212 at 50°C (59 mS $cm^{-1}$ for the membrane equilibrated at 50°C and 76% *RH*; dark blue line in Fig. 5b), the conductivity of the Tokuyama A201 is ≈3-fold lower (19 mS $cm^{-1}$ for the membrane equilibrated at 50°C and 80% *RH*), which can at least partially be ascribed to the difference of the ionic mobility between the hydroxide ion and the proton (factor of ≈1.8). Furthermore, we assume that the general structure/morphology of alkaline membranes is not yet fully optimized due to their novelty compared to the well-established Nafion 212 membrane. These structural/morphological differences could also be the reason for the similar conductivity of the Tokuyama A201 membrane and the here examined sulfonic acid membrane with a hydrocarbon backbone (15 mS $cm^{-1}$ for the membrane equilibrated at 50°C and 80% *RH*, see Fig. 6, dark blue lines), underlining the importance of a well-optimized membrane structure/morphology. Compared to the HC-PEM, the conductivity of the alkaline membrane in the hydroxide form decreases less strongly when lowering the *RH* below 50% (e.g., 6 mS $cm^{-1}$ vs 0.5 mS $cm^{-1}$ at 50°C for membranes equilibrated at 40% *RH* and 50°C). The reasonably high conductivity at low *RH* is an indicator for an upkeep of the desired phase separation to maintain well-percolating ion conduction pathways. Nevertheless, converting the hydroxide into the (bi-)carbonate form results in a much stronger decrease of the conductivity under these low *RH* conditions (0.6 mS $cm^{-1}$ at 50°C, see Fig. 8b, red lines), again comparable to the above values for the HC-PEM. The fact that the membrane conductivity in the (bi-)

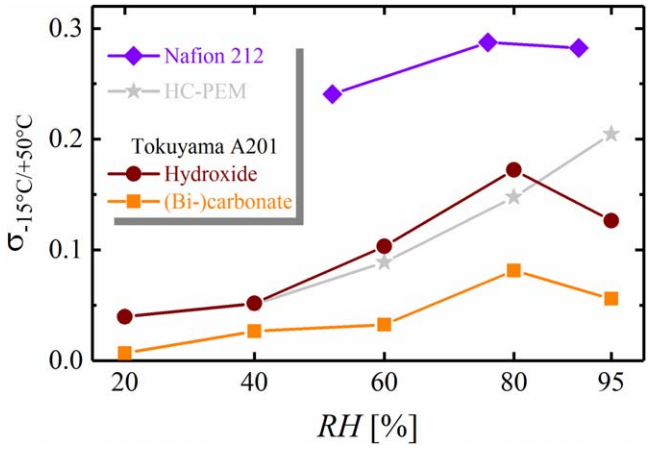


**Figure 9.** Ratio of the conductivity values measured at −15°C vs +50°C, $\sigma_{-15°C/+50°C}$, for Nafion 212, HC-PEM, and Tokuyama A201 in hydroxide and (bi-)carbonate form. All membranes were equilibrated at 50°C with $N_2/N_2$ humidified at different *RH* values, which are depicted in the figure (x-axis). $\sigma$ was calculated by subtraction of $R_{electr.}$ from the measured *HFR* and normalization to the thickness of the membrane according to Eq. 3. The hydroxide form was obtained by the carbonate purge approach described in Fig. 7, while the (bi-)carbonate form was obtained by a subsequent exposure to air/air.

carbonate form is one order of magnitude smaller compared to the hydroxide form at low water content might be a hint that the phase separation inside the Tokuyama A201 membrane is less effective in the (bi-)carbonate form compared to the hydroxide form.

The general trend of significantly decreasing conductivity with decreasing temperatures was comparable to that observed for PEMs. For example, for membranes equilibrated at 50°C and ≈80% *RH*, the conductivity decrease from 50°C to −15°C for Nafion 212 was from 60 to 16 mS $cm^{-1}$ (Fig. 5b, dark blue diamonds), for the HC-PEM it decreased from 15 to 2.2 mS $cm^{-1}$ (Fig. 6, dark blue circles), and for the Tokuyama A201 membrane it decreased from 20 to 3.5 mS $cm^{-1}$ for the hydroxide form (Fig. 8a, dark blue circles) and from 4.6 to 0.4 mS $cm^{-1}$ for the (bi-)carbonate form (Fig. 8a, dark blue circles). At a humidification level close to saturation, i.e., for equilibration at 50°C and 95% *RH*, a bend in the trend of decreasing conductivity was observed for both, the hydroxide and carbonate form (see light blue lines in Figs. 8a and b). We suspect that the more severe decrease of conductivity at ≈0°C in those measurements originates from freezing of liquid water in the membrane, causing, e.g., a blockage of ionic conduction pathways.

One interesting aspect is the much larger conductivity loss with temperature for the HC-PEM and the AEM (in the hydroxide form, and most pronouncedly in the (bi-)carbonate form), if compared to the Nafion 212 membrane. This is illustrated in Fig. 9, showing the ratio of the membrane conductivities at −15°C over that at +50°C ($\sigma_{-15°C}/\sigma_{+50°C}$) vs. the *RH* value at which the membranes were equilibrated at 50°C. Quite clearly, $\sigma_{-15°C}/\sigma_{+50°C}$ is significantly larger for the Nafion 212 membrane compared to the other membranes, meaning that its conductivity loss with decreasing temperature is less. This becomes particularly pronounced as the membrane water content decreases, i.e., for membrane equilibration at 50°C at ⩽60% *RH*. For example, for membranes equilibrated at 50°C and 60% RH, the loss of conductivity when lowering the temperature from +50°C to −15°C is ≈4-fold for Nafion 212 while it is ≈9-fold for the HC-PEM and for the AEM in the hydroxide form, and even ≈20-fold for the AEM in the (bi-)carbonate form. The origin of this behavior is unclear at this point, but it certainly points out the critical aspect of low temperature conductivity for HC-PEMs and for AEMs, particularly in their (bi-)carbonate form.

***Activation energy for ionic conduction.***—To obtain some more insights into the conduction properties of the different membranes at a given water content (adjusted by equilibration at +50°C at different *RH* values), the activation energy for ionic conduction was determined from the slope of a plot showing the logarithm of the product of conductivity and measurement temperature versus the inverse of the temperature, according to Eq. 6.

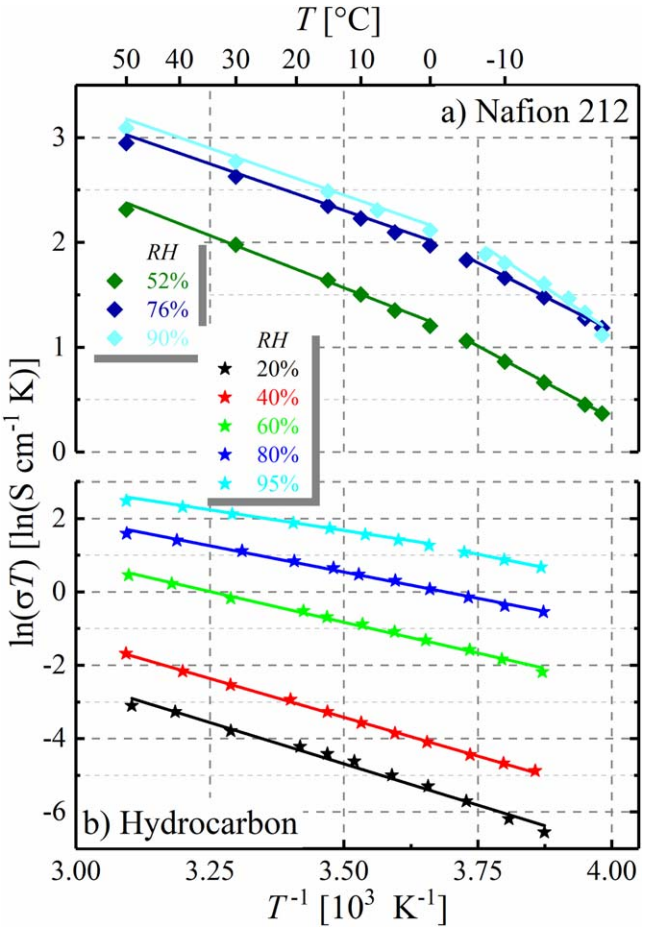


**Figure 10.** Arrhenius plot showing the logarithm of the product of temperature, *T*, and conductivity, $\sigma$, versus the inverse of the temperature (multiplied with 1000) for different membrane water contents obtained by equilibration of the membranes at +50°C with $N_2/N_2$ humidified at different *RH* values: (a) Nafion 212 and (b) a hydrocarbon-based HC-PEM. For conductivity ($\sigma$) measurements, the membranes were cooled down at the established membrane water content to the measurement temperature (data only shown for freeze cycle); $\sigma$ was calculated by subtraction of $R_{electr.}$ from the measured *HFR* and by normalization to the thickness of the membrane according to Eq. 3.

$$\ln(\sigma T) = \ln(\sigma_0) - \frac{E_A}{k_B} \cdot \frac{1}{T} \quad [6]$$

where $\sigma$ is the conductivity (in S $cm^{-1}$), *T* is the temperature (in K), $\sigma_0$ is the pre-exponential factor, $k_B$ is the Boltzmann constant ($8.617 \cdot 10^{-5}$ eV $K^{-1}$) and $E_A$ is the activation energy (in eV). This is shown in Fig. 10a for Nafion 212 (diamonds) and in Fig. 10b for the hydrocarbon-based HC-PEM (stars); the resulting $E_A$ values of all tested membranes are shown in Table I. Since no significant difference was found between the conductivity obtained during the freeze and during the thaw cycle for the chosen range of membrane water content (a hysteresis is commonly only observed for $\lambda \geqslant 12$),[26,36] only the freeze cycle conductivities are displayed in Fig. 10.

The data collected for Nafion 212 were fitted to a linear regression line, divided into one regime above 0°C and another one at lower temperatures, since a clear change of slope was observed below the freezing point of water. Even though this change

**Table I. Activation energy for the ionic membrane conduction (in units of eV) for different membrane water contents obtained by equilibration of the membranes at +50°C with $N_2/N_2$ humidified at the below specified different *RH* values (in %). Subsequently, the membranes were cooled down at the established membrane water content to different temperatures for conductivity ($\sigma$) measurement (data only shown for freeze cycles), whereby $\sigma$ was calculated by subtraction of $R_{electr.}$ from the measured *HFR* and by normalization to the thickness of the membrane according to Eq. 3. The activation energy ($E_A$) was extracted either over the entire temperature region (values displayed in the middle) or by fitting all values above and below the freezing point of water separately (values on the left and right, respectively).**

| Nafion 212 | | | HC-PEM | | | Tokuyama A201 ($OH^-$) | | | Tokuyama A201 ($HCO_3^-$) | | |
|---|---|---|---|---|---|---|---|---|---|---|---|
| *RH* | $E_A$ [eV] | | *RH* | $E_A$ [eV] | | *RH* | $E_A$ [eV] | | *RH* | $E_A$ [eV] | |
| | | | 20 | 0.39 | | 20 | 0.32 | 0.51 | 20 | 0.63 | |
| | | | 40 | 0.36 | | 40 | 0.31 | 0.43 | 40 | 0.45 | |
| 52 | 0.17 | 0.23 | 60 | 0.29 | | 60 | 0.25 | 0.34 | 60 | 0.35 | 0.52 |
| 76 | 0.15 | 0.22 | 80 | 0.25 | | 80 | 0.20 | 0.25 | 80 | 0.26 | 0.42 |
| 90 | 0.15 | 0.29 | 95 | 0.19 | 0.25 | 95 | 0.17 | 0.47 | 95 | 0.22 | 0.77 |

in slope is clearly visible at 0°C for the Nafion 212 data shown in Fig. 10a, it has to be mentioned that the demarcation of two different conduction regimes has been made at temperatures near but not exactly at 0°C by other authors.[36] Considering the linear fit above 0°C, we found a slightly increasing activation energy with decreasing water content for Nafion 212 (0.15, 0.15, and 0.17 eV at $\lambda = 8$, 6, and 4, respectively; see Table I), which is in good agreement with data presented in the literature (e.g., Thompson et al. found 0.19 and 0.22 eV at $\lambda = 8$ and 6, respectively).[36] Thompson et al. attributed the increasing activation energy for proton conduction at lower water content to a gradual change of the conduction mechanism from proton hopping according to the so-called Grotthus mechanism (similar to dilute acids), to a vehicular transport, requiring partial side-chain rearrangement. Similar to other researchers, we also observed an increase of the activation energy for the temperature regime below the freezing point of water (here between −6 and −23°C), being most significant at high $\lambda$ values (e.g., for equilibration at +50°C and 90% RH ($\lambda = 8$) from a value of 0.15 eV above the freezing point to 0.29 eV in the sub-freezing regime; see Table I). This again indicates a shift of the conduction mechanism due to the decreasing mobility in the ionomer phase as the water phase solidifies, while different transition temperatures for this process were reported in the literature.[36,42,43] However, it is commonly reported that the transition temperature shifts to lower values as the water content in the membrane decreases, explaining the less significant increase of $E_A$ at lower water content (e.g., 0.23 eV at $\lambda = 4$, obtained by equilibration at +50°C and 52% RH; see Table I).

In general, the trend of increasing $E_A$ with decreasing *RH* was also observed for the hydrocarbon-based HC-PEM, with values ranging in a similar order compared to Nafion 212, i.e., from 0.19 to 0.39 eV for membranes equilibrated at +50°C with $N_2/N_2$ humidified between 95 and 20% *RH* (see Table I). In contrast to Nafion 212, however, no difference in the slopes between temperatures above and below 0°C were observed, apart for equilibration at the highest *RH* (95%), where the activation energy increased from 0.19 eV at high temperature to 0.25 eV below the freezing point of water, similar to the behavior observed for Nafion 212. We hypothesize that the missing transition for most water contents for this type of membrane originates from a lower degree of phase separation even at comparably high *RH*, hence a less significant (or even absent) change of the conduction mechanism as the temperature decreases. This finding is in good agreement with the previously reported lower conductivity of this membrane determined in this study, especially at lower *RH*, where we assume that the proton conduction is strongly hindered.

The activation energy extracted from the conductivity data of the AEM in hydroxide form (Fig. 11a) also shows two different temperature regimes, roughly separated by the freezing point of water. Furthermore, the measured $E_A$ is similar to that of Nafion, increasing in the high-temperature regime from 0.17 to 0.32 eV as

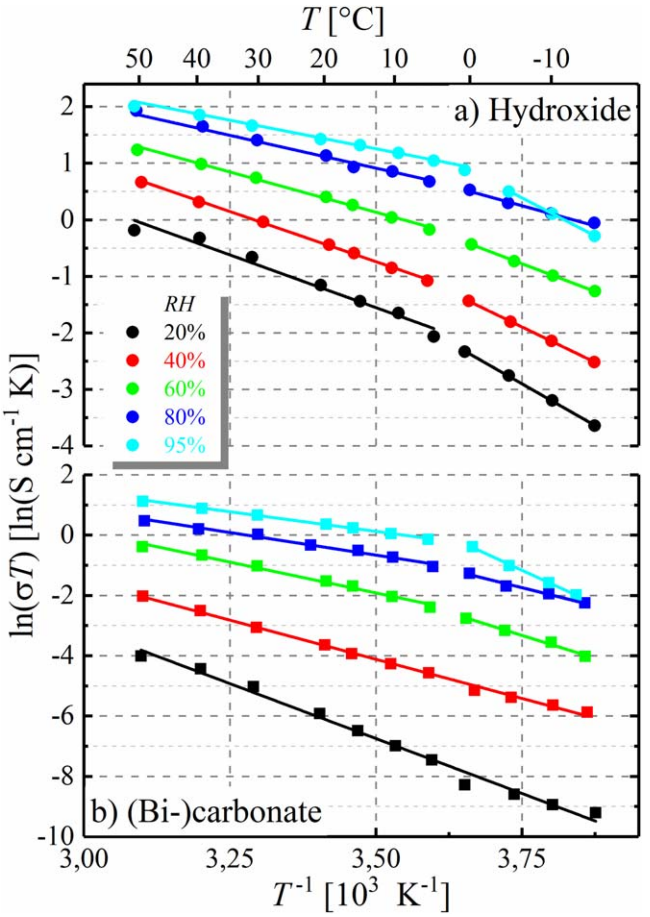


**Figure 11.** Arrhenius plot showing the logarithm of the product of temperature and conductivity versus the inverse of the temperature (multiplied with 1000) for different water contents of a Tokuyama A201 membrane obtained by equilibration of the membranes at +50°C with $N_2/N_2$ humidified at different *RH* values: (a) in its hydroxide form and (b) in its (bi-)carbonate form. For conductivity ($\sigma$) measurements, the membranes were cooled down at the previously established membrane water content to the measurement temperature (data only shown for freeze cycle): $\sigma$ was calculated by subtraction of $R_{electr.}$ from the measured *HFR* and by normalization to the thickness of the membrane according to Eq. 3.

the water content decreases (set by equilibration at +50°C with $N_2/N_2$ humidified at 95% to 20% *RH*), and increasing in the low temperature region and from 0.47 to 0.51 eV as the water content decreases (see Table I). First of all, these results indicate that the ion conduction mechanism is similar in the alkaline membrane and Nafion 212, i.e., at reasonably high water content, hydroxide ions in

the AEM can be transported by a mechanism similarly efficient as proton hopping in PEMs (while probably not completely analogous).[44] We conclude from the data, that this ion transport mechanism is impaired by vehicular transport as the water content decreases, indicated by the gradual increase of $E_A$, resulting in a lower conductivity at these conditions (Fig. 8a). This is also in line with the previously reported absence of a conductivity breakdown in the AEM for the hydroxide form at low *RH* (evident for the hydrocarbon-based membrane), where we assume that an interconnected network of the water phase can be reasonably well-maintained and that only a gradual change in the transport mechanism is present. Similar to Nafion 212, the activation energy increase when entering the low temperature regime is most significant for the highest water content, where the freezing of water in the membrane seems to strongly limit the mobility of the ionic species.

In contrast to the similarities between Nafion 212 and the Tokuyama A201 AEM in hydroxide form, the Arrhenius plot for the AEM in carbonate form (Fig. 11b) resembles a different picture. Similar to the hydrocarbon-based HC-PEM, a separation into two different regimes was only visible at high water contents (for equilibration at +50°C at $RH \geqslant 60\%$), with no change of slope below the freezing point of water at lower water content. This might either be due to a less distinct separation of hydrophilic and hydrophobic domains in carbonate form, similar to that observed for the hydrocarbon-based HC-PEM or to a generally higher need for a connected hydrophilic network to conduct carbonate and (bi-) carbonate ions compared to hydroxide ions or protons. While we cannot disprove either of the two hypothesis, we believe that the intrinsically lower mobility of (bi-)carbonate ions requires more well-connected ionic pathways for high membrane conductivity, which likely causes the absence of a transition temperature, rather than a change of the hydrophilicity in the same membrane when exchanging hydroxide with carbonate. Therefore, we conclude that the vehicular conduction mechanism plays a more significant role for AEMs in the carbonate form compared to an ion hopping mechanism, which is unlikely to occur for the rather bulky (bi-) carbonate ions. Nevertheless, the trend of increasing $E_A$ with decreasing water content (i.e., with decreasing equilibration *RH*) was also found for the (bi-)carbonate form, with $E_A$ increasing from 0.22 and 0.63 eV (95% and 20% *RH*) in the high temperature regime. In the low temperature regime below the freezing point of water, the activation energy at any given water content is substantially larger (see Table I); the very large activation energy observed in this region is of course reflected in the dramatic conductivity loss between +50°C and −15°C (≈20-fold) which is shown in Fig. 9.

***Implications of AEM conductivity for automotive applications.***—While the conductivity of the here examined AEM (Tokuyama A201) in the hydroxide form at 50°C and high relative humidity (≈20 mS cm$^{-1}$ at 95% RH, see Fig. 8a) is ≈3.5-fold lower than that of Nafion 212 (≈70 mS cm$^{-1}$ at 90% RH, see Fig. 5b), it would still afford a reasonably small voltage loss for a ≈10 $\mu$m thick membrane (a thickness used in today's PEM fuel cells for vehicles), namely ≈50 mV at 1 A cm$^{-2}$. More of a concern, however, is the dramatic conductivity loss for AEMs at sub-freezing conditions, which is much larger than for Nafion 212 (see Fig. 9), which might be critical for freeze-starting a fuel cell, particularly since this is generally preceded by equilibrating the fuel cell at low *RH* conditions in order to avoid the condensation of liquid water in the electrodes, diffusion media, and flow-fields. Exemplarily, one can estimate the membrane resistance losses at a fuel cell freeze start-up from −15°C at a current density of 0.1 A cm$^{-2}$ (certainly a lower limit for a reasonable start-up power) from the conductivities obtained at −15°C and intermediate water content for Nafion 212 (≈7 mS cm$^{-1}$; equilibrated at +50°C and 52% *RH*), the HC-PEM (≈0.4 mS cm$^{-1}$; equilibrated at +50°C and 60% *RH*) and the alkaline membrane in hydroxide (≈1 mS cm$^{-1}$; equilibrated at +50° C and 60% *RH*) or (bi-)carbonate form (≈0.07 mS cm$^{-1}$; equilibrated at +50°C and 60% *RH*), as shown in Figs. 5b, 6, and 8. For ≈10 $\mu$m thick membranes, the associated voltage drop would be roughly 0.01, 0.25, 0.10, and 1.4 V for Nafion 212, the HC-PEM, and the AEM in hydroxide or (bi-)carbonate form, respectively. A voltage loss of ≈1.4 V essentially means that a current of even 0.1 A cm$^{-2}$ at −15°C could not be drawn for the Tokuyama A201 membrane in its (bi-)carbonate form, likely preventing a successful freeze start-up; on the other hand, a freeze start-up at under these conditions would theoretically be achievable for in the hydroxide form. This implies that it would either be necessary to improve the conductivity of anionic membranes in the (bi-)carbonate form, or that one would have to assure that the AEM would remain in its hydroxide form during the shut-down and during extended shut-down times.

## Conclusions

In this study, we presented a method for the in-situ adjustment of the water content of fuel cell membranes by equilibration of the membranes at +50°C with $N_2/N_2$ humidified at different *RH* values, followed by a brief dry-gas purge which removes liquid water from the flow-field without significantly changing the membrane waer content. This way, the conductivity of membranes can be determined for a defined water content at low and sub-freezing temperatures by quantifying the electrical resistance and measuring the high frequency resistance (*HFR*). After validation of this methodology with a commercially available Nafion 212 membrane, the conductivity of a hydrocarbon-based PEM (HC-PEM) and of an AEM (Tokuyama A201) were determined. To disentangle the (bi-)carbonate and hydroxide form in the AEM, the MEA was subjected to an electrochemical pre-treatment followed by equilibration in the appropriate gas atmosphere.

The measurements showed that the conductivity of the here examined AEM and of the HC-PEM not only decreases significantly when the membrane water content decreases, but that their conductivity drops much more rapidly with decreasing temperature than that of a Nafion 212 membrane, particularly at intermediate and low water content. The latter effect is most strongly pronounced for the AEM in its (bi-)carbonate form, which has significant implications for the freeze start-up capability of alkaline membrane fuel cells.

## Acknowledgments

The supply of an alkaline membrane as comparison to the commercially available Tokuyama A201 by Kenneth Charles Neyerlin from the National Renewable Energy Laboratory (Denver, USA) is highly appreciated.

## ORCID

Jan N. Schwämmlein https://orcid.org/0000-0001-8902-4508

## References

1. Hyundai Motor Co. (accessed 02/24/2020), https://hyundai.de/downloads/modell_-prospekte/nexo_flyer_201803.pdf/.
2. Toyota Motor Co. (accessed 01/04/2019), https://toyota.com/content/ebrochure/2018/mirai_FuelCellTech.pdf.
3. Honda Motor Co. (accessed 10/18/2018), https://automobiles.honda.com/-/media/Honda-Automobiles/Vehicles/2017/Clarity-Fuel-Cell/Brochure/MY18_Clarity_FCV_Flyer.pdf.
4. J. Durst, C. Simon, F. Hasché, and H. A. Gasteiger, *J. Electrochem. Soc.*, **162**, F190 (2015).
5. U. A. Paulus, T. J. Schmidt, H. A. Gasteiger, and R. J. Behm, *J. Electroanal. Chem.*, **495**, 134 (2001).
6. B. Han, C. E. Carlton, A. Kongkanand, R. S. Kukreja, B. R. Theobald, L. Gan, R. O'Malley, P. Strasser, F. T. Wagner, and Y. Shao-Horn, *Energy Environ. Sci.*, **8**, 258 (2015).
7. A. Kongkanand and M. F. Mathias, *J. Phys. Chem. Lett.*, **7**, 1127 (2016).
8. N. Wagner, M. Schulze, and E. Gülzow, *J. Power Sources*, **127**, 264 (2004).
9. . Gamburzev, K. Petrov, and A. J. Appleby, *J. Appl. Electrochem.*, **32**, 805 (2002).
10. M. Schulze and E. Gülzow, *J. Power Sources*, **127**, 252 (2004).
11. J. R. Varcoe and R. C. T. Slade, *Fuel Cells.*, **5**, 187 (2005).
12. W. Sheng, H. A. Gasteiger, and Y. Shao-Horn, *J. Electrochem. Soc.*, **157**, B1529 (2010).

13. J. Durst, C. Simon, A. Siebel, P. J. Rheinländer, T. Schuler, M. Hanzlik, J. Herranz, F. Hasché, and H. A. Gasteiger, *ECS Trans.*, **64**, 1069 (2014).
14. J. Durst, A. Siebel, C. Simon, F. Hasché, J. Herranz, and H. A. Gasteiger, *Energy Environ. Sci.*, **7**, 2255 (2014).
15. P. J. Rheinländer, J. Herranz, J. Durst, and H. A. Gasteiger, *J. Electrochem. Soc.*, **161**, F1448 (2014).
16. M. D. Woodroof, J. A. Wittkopf, S. Gu, and Y. S. Yan, *Electrochem. Commun.*, **61**, 57 (2015).
17. G. F. McLean, T. Niet, S. Prince-Richard, and N. Djilali, *Int. J. Hydrogen Energ.*, **27**, 507 (2002).
18. . Gottesfeld, D. R. Dekel, M. Page, C. Bae, Y. Yan, P. Zelenay, and Y. S. Kim, *J. Power Sources*, **375**, 170 (2018).
19. G. Merle, M. Wessling, and K. Nijmeijer, *J. Membr. Sci.*, **377**, 1 (2011).
20. J. Fan et al., *Nat. Commun.*, **10**, 2306 (2019).
21. J. R. Varcoe et al., *Energy Environ. Sci.*, **7**, 3135 (2014).
22. A. Filpi, M. Boccia, and H. A. Gasteiger, *ECS Trans.*, **16**, 1835 (2008).
23. N. Ziv, A. N. Mondal, T. Weissbach, S. Holdcroft, and D. R. Dekel, *J. Membr. Sci.*, **586**, 140 (2019).
24. K. N. Grew, X. Ren, and D. Chu, *Electrochem. Solid-State Lett.*, **14**, B127 (2011).
25. Q. Duan, S. Ge, and C.-Y. Wang, *J. Power Sources*, **243**, 773 (2013).
26. E. L. Thompson, W. Gu, and H. A. Gasteiger, *Handbook of Fuel Cells*, ed. W. Vielstich, H. Yokokawa, and H. A. Gasteiger (John Wiley & Sons, Chichester) 1st ed., p. 699 (2009).
27. A. Albert, *Radiation-Grafted Polymer Electrolyte Membranes for Water Electrolysis* (Swiss Federal Institute of Technology Zurich, Zurich, Switzerland) Dissertation (2017).
28. C. K. Mittelsteadt and H. Liu, *Handbook of Fuel Cells*, ed. W. Vielstich, H. Yokokawa, and H. A. Gasteiger (John Wiley & Sons, Chichester) 1st ed., p. 345 (2009).
29. G. S. Harzer, J. N. Schwämmlein, A. M. Damjanović, S. Ghosh, and H. A. Gasteiger, *J. Electrochem. Soc.*, **165**, F3118 (2018).
30. J. N. Schwämmlein, G. S. Harzer, P. Pfändner, A. Blankenship, H. A. El-Sayed, and H. A. Gasteiger, *J. Electrochem. Soc.*, **165**, J3173 (2018).
31. C. Simon, F. Hasché, and H. A. Gasteiger, *J. Electrochem. Soc.*, **164**, F591 (2017).
32. Y. Liu, M. W. Murphy, D. R. Baker, W. Gu, C. Ji, J. Jorne, and H. A. Gasteiger, *J. Electrochem. Soc.*, **156**, B970 (2009).
33. K. Tajiri, Y. Tabuchi, and C.-Y. Wang, *J. Electrochem. Soc.*, **154**, B147 (2007).
34. S. Watanabe, K. Fukuta, and H. Yanagi, *ECS Trans.*, **33**, 1837 (2010).
35. M. F. Mathias, J. Roth, J. Fleming, and W. Lehnert, *Handbook of Fuel Cells*, ed. W. Vielstich, A. Lamm, and H. A. Gasteiger (John Wiley & Sons, Chichester) 1st ed., p. 517 (2009).
36. E. L. Thompson, T. W. Capehart, T. J. Fuller, and J. Jorne, *J. Electrochem. Soc.*, **153**, A2351 (2006).
37. K. D. Kreuer, *Handbook of Fuel Cells*, ed. W. Vielstich, A. Lamm, and H. A. Gasteiger (John Wiley & Sons, Chichester) 1st ed., p. 420 (2009).
38. W.-J. Ahn, S.-D. Yim, Y.-W. Choi, Y.-J. Sohn, S.-H. Park, Y.-G. Yoon, G.-G. Park, T.-H. Yang, and K.-B. Kim, *Electrochim. Acta*, **56**, 7732 (2011).
39. S. Sitch et al., *Global Change Biol.*, **14**, 2015 (2008).
40. T. D. Myles, K. N. Grew, A. A. Peracchio, and W. K. S. Chiu, *J. Power Sources*, **296**, 225 (2015).
41. T. Kimura and Y. Yamazaki, *Electrochemistry.*, **79**, 94 (2011).
42. M. Cappadonia, J. W. Erning, and U. Stimming, *J. Electroanal. Chem.*, **376**, 189 (1994).
43. M. Cappadonia, J. W. Erning, S. M. Saberi Niaki, and U. Stimming, *Solid State Ionics*, **77**, 65 (1995).
44. M. E. Tuckerman, D. Marx, M. Parrinello, and M. E. Tuckerman, *Nature*, **417**, 925 (2002).